p-ISSN 2089 – 0133 e-ISSN 2477-6416 Indonesian Journal of Applied Physics (IJAP) Vol. 16 No. 1 page 76
URL : https://jurnal.uns.ac.id/ijap/article/view/117075 DOI : https://doi.org/10.13057/ijap.v16i1.117075

POPULATION REDISTRIBUTION IN A CONTINUOUSLY DRIVEN Λ-TYPE SEMICONDUCTOR QUANTUM DOT: ROLES OF RELAXATION-PATH ASYMMETRY AND OFF-RESONANT COUPLING

Arik Ramadhan, Bintoro S. Nugroho*, Asifa Asri, Azrul Azwar, Yudha Arman
Program Studi Fisika, Fakultas Matematika dan Ilmu Pengetahuan Alam, Universitas Tanjungpura, Pontianak, Indonesia
*b.s.nugroho@physics.untan.ac.id

Received 2026-04-02, Revised 2026-05-12, Accepted 2026-06-02,
Available Online, Published Regularly June 2026

ABSTRACT

Semiconductor quantum dots (SQDs) exhibit optical responses that are strongly influenced by their internal level structure, relaxation pathways, and excitation intensity. This study investigates the time- and intensity-dependent population dynamics of a continuously driven single Λ-type three-level SQD using the density-matrix formalism within the rotating-wave approximation. Dissipative processes are incorporated through Lindblad-type relaxation terms, while the transient and stationary responses are obtained, respectively, by numerical time integration and steady-state solution of the density-matrix equations. Special attention is given to the relaxation channel γ_{32} and the off-resonant transition dipole moment μ_{32}. The results show that γ_{32} primarily controls the transient redistribution route and the timescale required to reach the stationary regime, whereas the early oscillatory behavior remains dominated by the resonantly driven $|1\rangle \leftrightarrow |3\rangle$ transition. In the steady-state regime, γ_{32} mainly determines how population leaving the upper state is partitioned between the two lower states, while μ_{32} governs how readily the off-resonant $|2\rangle \leftrightarrow |3\rangle$ branch becomes active as the driving intensity increases. Consequently, the crossover from predominantly resonant two-level-like behavior to genuine three-level population redistribution is controlled by the combined action of relaxation-path asymmetry and off-resonant coupling strength. These findings provide a clearer mechanism-based interpretation of driven population redistribution in effective multilevel SQD systems.

Keywords: continuous-wave excitation; density-matrix formalism; population dynamics; semiconductor quantum dots; Λ-type three-level system

INTRODUCTION

Semiconductor quantum dots (SQDs) are important materials systems due to their quantum confinement, which produces discrete energy structures and strongly size-dependent optical properties. These features support the use of SQDs in optoelectronics, sensing, and quantum photonics. They also provide a valuable platform for studying light-matter interactions in confined semiconductor systems [1–4]. The optical response of a QD is governed not only by its spectral resonance, but also by how its internal level structure and relaxation pathways redistribute population under external excitation.

A central issue in driven SQD systems is the time-dependent population dynamics. Under coherent optical excitation, the populations of quantum states evolve through the competition between field-induced transitions and dissipative channels, rather than following the applied field instantaneously. This transient behavior is directly relevant to coherent control and optical manipulation of semiconductor excitations. Recent studies have shown that driven SQDs can exhibit phonon-assisted population inversion [5], damped and intensity-dependent coherent oscillations [6-7], prolonged coherent optical response [8], and signatures of dynamically dressed states [9]. More broadly, coherent spectroscopic studies have established that the optical response of semiconductor nanostructures is highly sensitive to relaxation and dephasing processes [10].

In addition to transient dynamics, the optical response of SQDs is strongly affected by excitation intensity. As the driving field increases, nonlinear effects can reshape the population distribution, induce saturation, and activate transitions that remain weak in the low-intensity regime. Such behavior has been reported in direct two-photon excitation of SQDs [11], in quantum-dot molecules showing tunneling-induced optical limiting [12], in quantum-dot supercrystals exhibiting nonlinear collective response [13], and in hybrid nanostructures involving metallic nanoparticles or graphene nanodisks [14–16]. These studies show that the driven response of semiconductor nanostructures is determined not only by resonance conditions but also by the interplay among transition strength, relaxation pathways, and field amplitude.

At the same time, the optical behavior of SQDs depends sensitively on the detailed material realization. Wetting-layer effects can modify the excitonic structure [17], recombination dynamics depend on the specific decay routes available in the SQD system [18-19], and coherence can be tuned in engineered semiconductor structures [20]. For this reason, simplified few-level models remain useful for transparently isolating physically meaningful mechanisms. In SQDs, such models can represent idealized multilevel excitonic structures in which optical driving competes with internal relaxation. Within this context, the physically important question is not merely how a multilevel SQD responds to light in general, but what controls the crossover from resonantly driven two-level-like behavior to genuine three-level population redistribution under continuous-wave excitation.

The underlying mechanism remains insufficiently resolved for a continuously driven single Λ-type three-level SQD, particularly regarding the distinct and combined roles of relaxation-path asymmetry and off-resonant coupling strength. Previous studies have demonstrated rich driven behavior in SQDs and related hybrid nanostructures, including nonlinear optical response, coherent preparation, and multilevel effects in coupled systems [13–15,21]. However, a clear mechanism-based account of how the relaxation channel from the upper state and the dipole strength of the off-resonant transition jointly govern the transient redistribution route, the stationary population balance, and the onset of intensity-driven three-level participation in a single Λ-type SQD is still lacking. This issue is physically important because the Λ-type structure introduces an additional redistribution pathway that can shift the system away from a predominantly resonant two-level-like response and into a genuine three-level population regime under continuous-wave excitation.

To address this problem, the present work investigates the time- and intensity-dependent population dynamics of a single Λ-type SQD driven by a continuous-wave optical field. The analysis is based on the density-matrix formalism within the rotating-wave approximation, with dissipation incorporated through Lindblad-type relaxation terms. Special attention is given to the effective relaxation channel γ_{32}, which controls the redistribution of population from the upper state, and to the transition dipole moment μ_{32}, which determines how readily the off-resonant branch becomes active as the driving intensity increases. The objective is to clarify how these two parameters separately and jointly control the transient relaxation pathway, the stationary population distribution, and the crossover from predominantly resonant two-level-like dynamics to three-level population redistribution. The present analysis contributes by separating two physically distinct control mechanisms in a continuously driven effective Λ-type SQD, within the parameter range considered. Relaxation-path asymmetry, introduced by varying γ_{32} relative to γ_{31}, primarily determines how the population is redistributed and where the stationary population balance is established. The off-resonant coupling strength has a different role. Parameterized by the transition dipole moment μ_{32}, it sets the intensity scale at which the third level begins to participate effectively in the optical response. Hence, the present study provides a mechanism-oriented interpretation of driven population dynamics in an effective multilevel semiconductor SQD model and offers a clearer physical basis for understanding redistribution effects in more complex quantum-dot systems.

METHOD

This work employs the density-matrix formalism to study the population dynamics of a single Λ-type three-level semiconductor quantum dot driven by a classical continuous-wave field. The analysis proceeds in three stages. First, the physical system is represented as a driven dissipative three-level model with two optically allowed transitions and three relaxation channels. Second, the equations of motion for the density-matrix elements are derived from the master equation within the rotating-wave approximation (RWA). Third, the resulting equations are treated using two complementary numerical procedures: time-domain integration for the transient response and linear steady-state analysis for the stationary populations. The numerical calculations were performed in Python. The time-dependent equations were integrated using the RK45 solver from the SciPy library, whereas the steady-state algebraic system was solved using NumPy linear-algebra routines. The former was used to track the transient evolution of the populations and coherences, whereas the latter was used to determine the stationary solution directly. These methods are used here as established theoretical and numerical tools; the contribution of the present work lies in using them to isolate the distinct roles of relaxation-path asymmetry and off-resonant coupling strength in the population redistribution mechanism.

Theoretical Model

We consider a single SQD of radius r embedded in vacuum and driven by a linearly polarized monochromatic continuous wave (CW) electric field, $E(t) = E_0 \, cos \, cos \, (\omega t)$, where E_0 and ω denote the field amplitude and angular frequency, respectively [Figure 1(a)]. The SQD is modeled as a Λ-type three-level system consisting of the states $|1\rangle$, $|2\rangle$, and $|3\rangle$, with corresponding energies 0, $\hbar\omega_2$, and $\hbar\omega_3$. The optically allowed transitions are $|1\rangle \leftrightarrow |3\rangle$ and $|2\rangle \leftrightarrow |3\rangle$, with transition dipole moments $\mu_{31} = \mu_{13}$ and $\mu_{32} = \mu_{23}$, respectively, whereas the $|1\rangle \leftrightarrow |2\rangle$ transition is assumed to be dipole forbidden [Figure 1(b)]. In the present work, the level energies, transition dipole moments, and relaxation rates are treated as effective parameters representing the optical characteristics of the SQD.

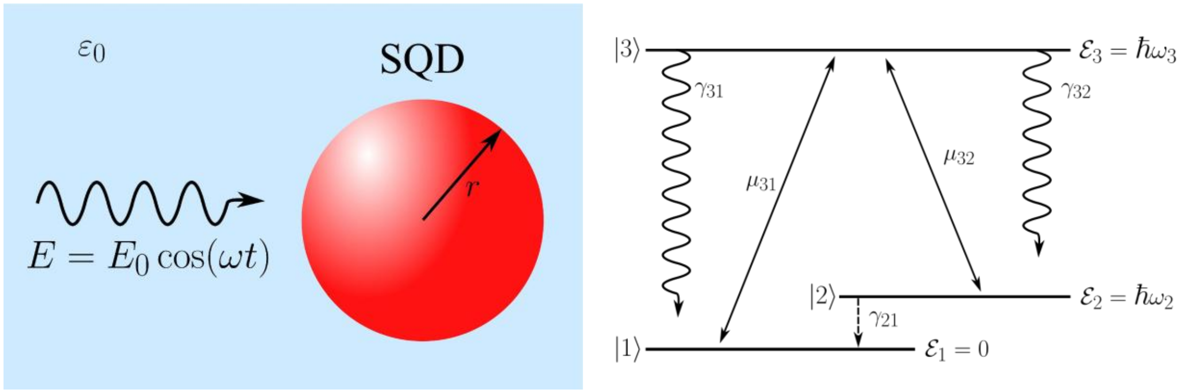

(a) (b)

Figure 1. (a) Schematic illustration of a single SQD driven by a linearly polarized continuous-wave electric field. (b) Energy-level diagram of the effective Λ-type three-level SQD model. The wavy arrows denote relaxation from the upper state $|3\rangle$ to the lower states $|1\rangle$ and $|2\rangle$, while the dashed arrow indicates relaxation from $|2\rangle$ to $|1\rangle$.

Because the SQD radius is assumed to be much smaller than the optical wavelength, i.e. $r \ll \lambda$, the spatial variation of the applied field across the SQD is neglected under the quasistatic approximation. Consequently, the electric field is treated as spatially uniform inside the SQD. For simplicity, the transition dipole moments are assumed to be parallel to each other and to the polarization direction of the incident field, so that the dipole interaction can be treated in scalar form.

Three relaxation channels are included to describe population relaxation, as indicated in Figure 1(b): $|3\rangle \to |1\rangle$ with rate γ_{31}, $|3\rangle \to |2\rangle$ with rate γ_{32}, and $|2\rangle \to |1\rangle$ with rate γ_{21}. In the present model, γ_{31} and γ_{32} describe relaxation from the upper state $|3\rangle$ to the two lower states, whereas γ_{21} is introduced as an effective lower-level relaxation channel that phenomenologically accounts for population transfer from $|2\rangle$ to $|1\rangle$. Accordingly, γ_{21} is not treated as a primary radiative decay channel, but rather as an effective dissipative process between the two lower states.

Master Equation in the Rotating-Wave Approximation

The population dynamics of the driven SQD are described within the density-matrix formalism. In the rotating frame with angular frequency ω of the applied field, the master equation is written as [22]

$$\dot{\hat{\rho}} = -\frac{i}{\hbar}\left[\hat{H}^{RWA}, \hat{\rho}\right] + \hat{L}(\hat{\rho}), \tag{1a}$$

where the overdot denotes the time derivative, H_{RWA} is the SQD Hamiltonian in the RWA, and $\hat{L}(\hat{\rho})$ is the Lindblad operator describing the relaxation processes.

The Hamiltonian in the RWA takes the form

$$\hat{H}^{RWA} = \hbar(\Delta_{21}\hat{\sigma}_{22} + \Delta_{31}\hat{\sigma}_{33}) - \frac{\hbar}{2}(\Omega_{31}\hat{\sigma}_{31} + \Omega_{32}\hat{\sigma}_{32} + H.c.) \tag{1b}$$

and the Lindblad operator is given by

$$\hat{L}(\hat{\rho}) = \frac{1}{2}\gamma_{31}([\hat{\sigma}_{13}\hat{\rho},\hat{\sigma}_{31}] + [\hat{\sigma}_{13},\hat{\rho}\hat{\sigma}_{31}]) + \frac{1}{2}\gamma_{32}([\hat{\sigma}_{23}\hat{\rho},\hat{\sigma}_{32}] + [\hat{\sigma}_{23},\hat{\rho}\hat{\sigma}_{32}]) + \frac{1}{2}\gamma_{21}([\hat{\sigma}_{12}\hat{\rho},\hat{\sigma}_{21}] + [\hat{\sigma}_{12},\hat{\rho}\hat{\sigma}_{21}]), \tag{1c}$$

where $\hat{\sigma}_{nm} = |n\rangle\langle m|$ with $m, n = 1, 2, 3$ is the transition operator, $\Delta_{21} = \omega_2 - \omega_1$ denotes the frequency of energy splitting between the two lower states, and $\Delta_{31} = \omega_3 - \omega$ is the detuning of the incident field from the $|1\rangle \leftrightarrow |3\rangle$ transition, while $\Omega_{31} = \mu_{31}E_0/\hbar$ and $\Omega_{32} = \mu_{32}E_0/\hbar$ are the Rabi frequencies associated with the two optically allowed transitions. It should be noted that, in Eq. (1c), the pure-dephasing terms are neglected to isolate the role of population relaxation and redistribution pathways in the driven dynamics.

The equations of motion for the density matrix elements obtained from projecting the master equation onto the basis states $\dot{\rho}_{nm} = \langle n|\,\dot{\hat{\rho}}\,|m\rangle$

$$\dot{\rho}_{11} = \frac{i\Omega_{31}}{2}(\rho_{31} - \rho_{13}) + \gamma_{21}\rho_{22} + \gamma_{31}\rho_{33}, \tag{2a}$$

$$\dot{\rho}_{22} = \frac{i\Omega_{32}}{2}(\rho_{32} - \rho_{23}) - \gamma_{21}\rho_{22} + \gamma_{32}\rho_{33}, \tag{2b}$$

$$\dot{\rho}_{33} = -\frac{i\Omega_{31}}{2}(\rho_{31} - \rho_{13}) - \frac{i\Omega_{32}}{2}(\rho_{32} - \rho_{23}) - \rho_{33}(\gamma_{31} + \gamma_{32}), \tag{2c}$$

$$\dot{\rho}_{31} = -\left[i\Delta_{31} + \frac{1}{2}(\gamma_{31} + \gamma_{32})\right]\rho_{31} + \frac{i\Omega_{32}}{2}\rho_{21} - \frac{i\Omega_{31}}{2}(\rho_{33} - \rho_{11}), \tag{2d}$$

$$\dot{\rho}_{32} = -\left[i(\Delta_{31} - \Delta_{21}) + \frac{1}{2}(\gamma_{31} + \gamma_{32} + \gamma_{21})\right]\rho_{32} + \frac{i\Omega_{31}}{2}\rho_{12} - \frac{i\Omega_{32}}{2}(\rho_{33} - \rho_{22}), \tag{2e}$$

$$\dot{\rho}_{21} = \frac{i\Omega_{32}}{2}\rho_{31} - \frac{i\Omega_{31}}{2}\rho_{23} - \left(i\Delta_{21} + \frac{1}{2}\gamma_{21}\right)\rho_{21}. \tag{2f}$$

The diagonal elements ρ_{11}, ρ_{22}, and ρ_{33} represent the populations of states $|1\rangle$, $|2\rangle$, and $|3\rangle$, respectively, whereas the off-diagonal elements represent the corresponding quantum coherences. Note that $\rho_{nm} = \rho^*_{mn}$ due to hermiticity of $\hat{\rho}$, thus equations (2a)-(2f) suffice to describe the dynamics of the density matrix.

Steady-State Solution

To characterize the stationary population response of the SQD under continuous-wave excitation, the time derivatives of all density-matrix elements in Eqs. (2a)-(2f) are set to zero, i.e. $\dot{\rho}_{nm} = 0$ With this assumption, the transient evolution is no longer considered, and the system is described by a time-independent solution in the rotating frame under continuous-wave excitation. As a result, the original set of coupled differential equations is transformed into a set of simultaneous algebraic equations for the steady-state density-matrix elements.

To complete the solution, the algebraic system is supplemented by the normalization requirement

$$\rho_{11} + \rho_{22} + \rho_{33} = 1, \tag{3}$$

which enforces conservation of total probability. Because this relation makes one of the population equations redundant, one diagonal equation is replaced by the normalization condition. The steady-state problem can then be written compactly as

$$MR = B, \tag{4}$$

where M denotes the matrix of coefficients, R contains the unknown steady-state density-matrix elements, and B represents the corresponding inhomogeneous term. For each selected set of excitation and model parameters, the steady-state density-matrix elements are obtained numerically using a direct linear solver. The numerical solution is then verified by checking that the normalization condition $\rho_{11} + \rho_{22} + \rho_{33} = 1$ is satisfied.

Parameterization and Physical Conditions

Unless otherwise stated, the calculations were performed using the representative parameter set $\hbar\Delta_{21} = 1\, meV$, $\mu_{31} = 0.9\, e\, nm$, $\gamma_{31} = 3\, ns^{-1}$, and $\gamma_{21} = 0.01\gamma_{31}$. These values are introduced as representative effective scales for a semiconductor quantum-dot system and are intended to clarify the mechanism of population redistribution rather than to reproduce a specific experimental material platform. The parameters γ_{32} and μ_{32} are treated as variable quantities to examine the effects of the additional relaxation pathway and the off-resonant optical coupling strength, respectively.

Before the optical field is applied, the system is assumed to be in its ground state. Accordingly, the initial conditions for the time-dependent calculations are taken as $\rho_{11}(0) = 1$, $\rho_{22}(0) = 0$, and $\rho_{33}(0) = 0$, while all coherence terms are initially set to zero. The calculations are performed under resonance with the $|1\rangle \leftrightarrow |3\rangle$ transition, so that $\Delta_{31} = 0$. In the intensity-dependent analysis, the driving-field intensity, $I = c\varepsilon_0 E_0^2/2$, where c is the speed of light and ε_0 is the vacuum permittivity, is varied through the field amplitude E_0. Since $\Omega_{31} = \mu_{31}E_0/\hbar$ and $\Omega_{32} = \mu_{32}E_0/\hbar$, both Rabi frequencies increase linearly with the applied field amplitude.

RESULTS AND DISCUSSION

Time-Dependent Response

The transient population dynamics were obtained by numerically integrating Eqs. (2a)–(2f) using the RK45 method. The system is initially assumed to occupy the ground state at $t = 0$. In addition to the parameter set introduced in the previous section, the calculations were performed at $I = 20\, W\, cm^{-2}$. Since the applied field is resonant with the $|1\rangle \leftrightarrow |3\rangle$ transition, the time-dependent response is determined by the competition among resonant optical excitation, relaxation from the upper state, and population redistribution through the additional channel γ_{32}. Throughout this subsection, μ_{32} is kept fixed while γ_{32} is varied to reveal the role of relaxation-path asymmetry in the transient dynamics.

Figure 2 shows the time evolution of the populations for three representative values of γ_{32}. The main result is that γ_{32} does not primarily alter the initial oscillatory exchange driven by the resonant $|1\rangle \leftrightarrow |3\rangle$ branch, but instead modifies the transient redistribution route by which the system approaches its stationary population distribution. This distinction is important because the optical field is resonant with the $|1\rangle \leftrightarrow |3\rangle$ transition, whereas the $|2\rangle \leftrightarrow |3\rangle$ branch enters the dynamics indirectly through relaxation from $|3\rangle$ and through the finite off-resonant coupling retained in the model.

For the case shown in Figure 2(a), the populations ρ_{11} and ρ_{33} exhibit damped oscillations at early times, whereas ρ_{22} increases monotonically without a pronounced oscillatory signature. This behavior follows directly from Eqs. (2a)-(2c): the resonant term involving Ω_{31} drives the coherent exchange between $|1\rangle$ and $|3\rangle$, while the population of $|2\rangle$ is fed mainly through the relaxation term $\gamma_{32}\rho_{33}$ in Eq. (2b). Because $|2\rangle$ is not resonantly driven under the chosen condition $\Delta_{31} = 0$, its occupation builds up predominantly as a secondary relaxation product rather than through direct coherent cycling. The damping of the oscillation in ρ_{11} and ρ_{33} originates from the irreversible loss terms associated with γ_{31} and γ_{32}, which gradually suppress the coherent exchange sustained by the resonant branch.

The damped oscillatory behavior found here is consistent with earlier reports of coherent Rabi-type oscillations and their damping in driven semiconductor quantum dots and related nanostructures [6-7]. The present analysis further shows that the additional relaxation channel γ_{32} primarily modifies the transient redistribution route and the timescale for reaching the stationary regime, rather than the oscillation frequency itself.

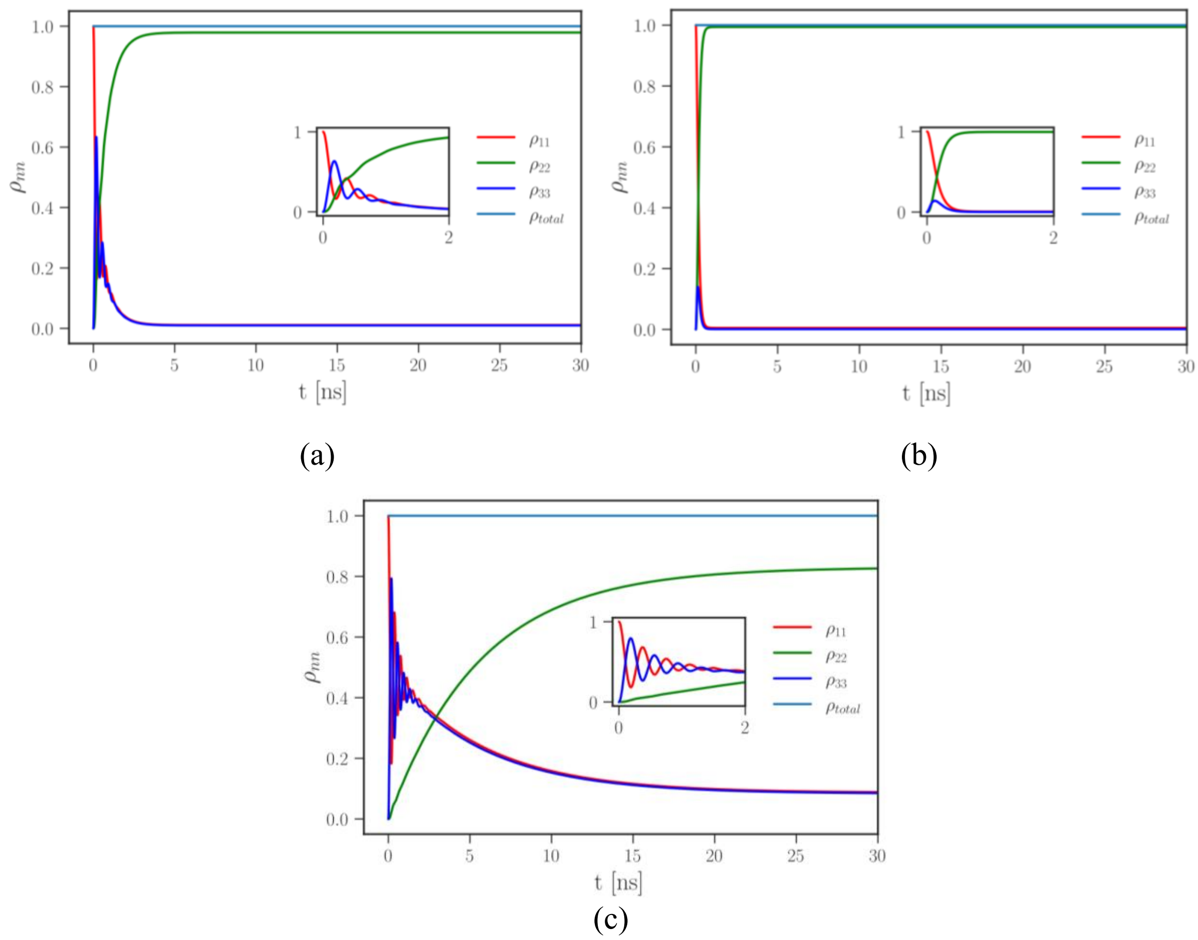

Figure 2. Transient populations ρ_{11}, ρ_{22}, and ρ_{33} of the driven Λ-type SQD for three representative values of γ_{32}: (a) $\gamma_{32} = \gamma_{31}$, (b) $\gamma_{32} = 10\gamma_{31}$, and (c) $\gamma_{32} = 0.1\gamma_{31}$. The calculations are performed under resonance with the $|1\rangle \leftrightarrow |3\rangle$ transition, with the remaining parameters fixed as specified in the text. In each panel, ρ_{11} is shown as a reference, and the inset highlights the early-time oscillatory behavior of ρ_{11} and ρ_{33}.

This mechanism becomes clearer when γ_{32} is increased. In Figure 2(b), the system reaches the stationary regime more rapidly than in Figure 2(a). The reason is that a larger γ_{32} enhances the transfer of population from $|3\rangle$ to $|2\rangle$, thereby accelerating the redistribution away from the resonantly coupled $|1\rangle \leftrightarrow |3\rangle$ subsystem. In other words, the additional decay path does not create the oscillation itself; rather, it drains population from the upper level and shortens the time over which the resonant pair $|1\rangle$ and $|3\rangle$ can sustain noticeable coherent exchange. Consequently, the stationary state is reached sooner, and the transient pathway becomes more strongly biased toward accumulation in $|2\rangle$.

A different transient scenario appears in Figure 2(c), where γ_{32} is smaller than γ_{31}. In this regime, the system behaves in an effectively two-level-like manner at early times, as indicated by the dominant oscillatory exchange between $|1\rangle$ and $|3\rangle$ in the inset, followed by a more gradual redistribution into $|2\rangle$. Physically, once the population reaches $|3\rangle$, the channel $|3\rangle \rightarrow |2\rangle$ is less efficient than the return path $|3\rangle \rightarrow |1\rangle$. The early-time dynamics, therefore, remain governed more strongly by the resonantly driven pair, while the transfer into the lower state $|2\rangle$ proceeds more slowly. Because the relaxation $|2\rangle \rightarrow |1\rangle$ is comparatively weak, $|2\rangle$ it still acts as a population reservoir, but its population builds up more slowly and reaches a lower stationary value than in the cases shown in Figures 2(a) and 2(b). This explains why the approach to the stationary state is prolonged and why the transient response retains a more pronounced two-level-like character.

An important point is that changing γ_{32} mainly affects the relaxation pathway and the timescale of the transient response, rather than the oscillation frequency itself. The early oscillatory behavior is still set primarily by the resonantly driven $|1\rangle \leftrightarrow |3\rangle$ transition through Ω_{31}, while γ_{32} controls how efficiently the population is diverted from the upper state into the second lower level $|2\rangle$. A larger γ_{32} accelerates this redistribution and shortens the transient evolution, whereas a smaller γ_{32} preserves the two-level-like character for longer times and delays the accumulation of population in $|2\rangle$. Thus, the time-domain analysis shows that relaxation-path asymmetry is the key factor governing how the system evolves from an initially resonant two-level-like response into a stationary three-level population distribution. This behavior follows from the different roles of the coherent and dissipative terms in Eqs. (2a)-(2f). The early exchange between $|1\rangle$ and $|3\rangle$ is driven directly by the resonant Rabi coupling Ω_{31}, whereas γ_{32} enters as an irreversible transfer channel through the term $\gamma_{32}\rho_{33}$ in Eq. (2b). The same relaxation rate also contributes to the decay of the optical coherence ρ_{31} through the total upper-state decay term in Eq. (2d). Thus, increasing γ_{32} mainly accelerates damping and population transfer from $|3\rangle$ to $|2\rangle$, rather than introducing a new coherent oscillation.

Intensity-Dependent Response

The stationary population response was obtained by solving the steady-state form of Eqs. (2a)-(2f), together with the normalization condition in Eq. (3). In this part of the analysis, the driving-field intensity is varied through the field amplitude E_0, while the system remains under resonance with the $|1\rangle \leftrightarrow |3\rangle$ transition, i.e. $\Delta_{31} = 0$. Under this condition, the intensity dependence of the stationary populations reflects how the resonantly driven branch gradually evolves from a predominantly two-level-like response into a three-level redistribution regime when the off-resonant channel becomes increasingly accessible. The respective roles of γ_{32} and μ_{32} are examined separately to distinguish the influence of relaxation-path asymmetry from that of off-resonant coupling strength.

Figure 3(a) shows the steady-state populations as functions of intensity for a fixed value of μ_{32} and a representative relaxation configuration. At very low intensity, the system remains almost entirely in the ground state, with $\rho_{11} \approx 1$, because the resonant driving is too weak to induce substantial population transfer. As the intensity increases, the resonantly driven transition $|1\rangle \leftrightarrow |3\rangle$ becomes more effective, leading to a decrease in ρ_{11} and a corresponding increase in ρ_{33}, while ρ_{22} also starts to build up through the relaxation pathway fed from the upper state. In this regime, the population accumulation in $|2\rangle$ is still limited because the $|2\rangle \leftrightarrow |3\rangle$ branch remains off-resonant and therefore contributes only weakly.

A more distinct redistribution emerges at higher intensity, when the optical coupling associated with the off-resonant branch becomes sufficiently strong to compete with the lower-level splitting. From Figure 3(a), this crossover appears to start around $I \approx 10^{4.4}\, W\, cm^{-2}$, where $\hbar\Omega_{32}$ becomes comparable to the energy separation between the two lower states, causing the $|2\rangle \leftrightarrow |3\rangle$ transition to become increasingly active. The system then crosses over from a response dominated mainly by the resonant $|1\rangle \leftrightarrow |3\rangle$ branch to a regime in which all three states participate more actively in the stationary population balance. This crossover is reflected by the reduction of ρ_{22} at higher intensity and by the accompanying redistribution of population among the three levels. Thus, the main effect of increasing intensity is not merely stronger excitation, but the activation of an additional population-transfer route that is weak in the low-intensity limit, marking the onset of genuine three-level participation in the stationary response.

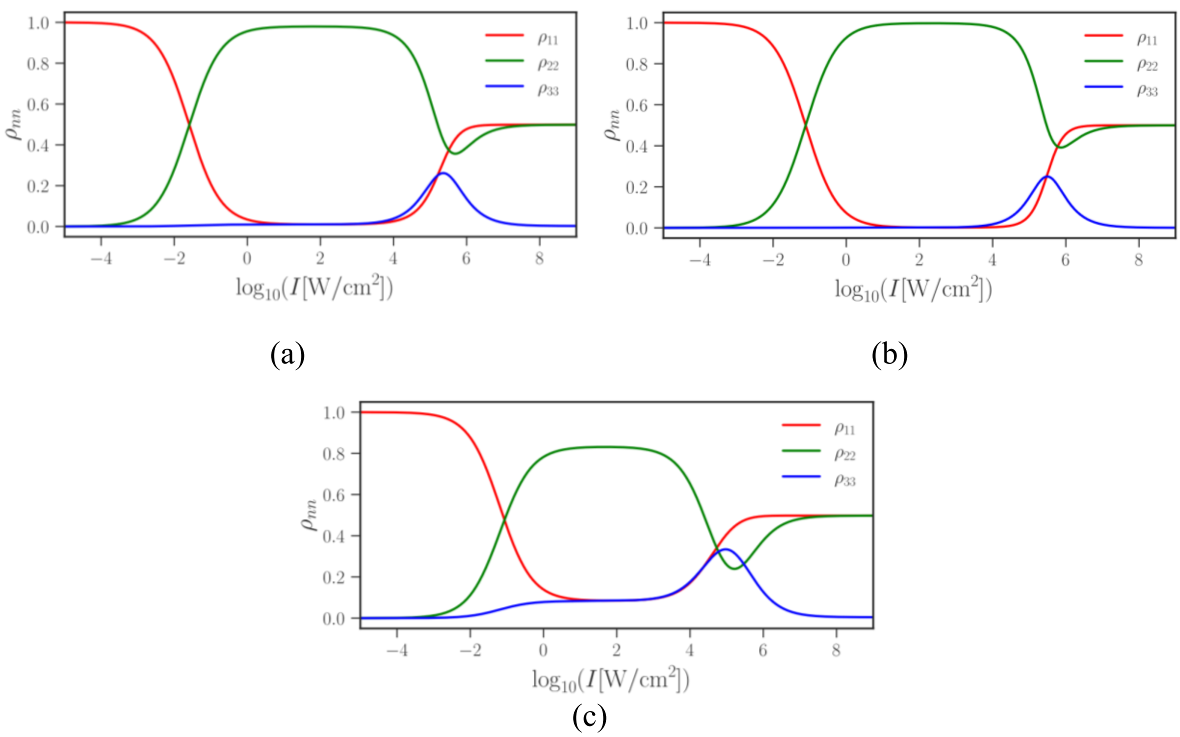

Figure 3. Steady-state populations ρ_{11}, ρ_{22}, and ρ_{33} as functions of the driving-field intensity for fixed $\mu_{32} = \mu_{31}$ and three representative values of γ_{32}: (a) $\gamma_{32} = \gamma_{31}$, (b) $\gamma_{32} = 10\gamma_{31}$, and (c) $\gamma_{32} = 0.1\gamma_{31}$. The system is driven under resonance with the $|1\rangle \leftrightarrow |3\rangle$ transition, and all other parameters are kept as given in the text.

This result indicates that the intensity dependence is not simply a monotonic increase of excitation strength. At low intensity, the system remains close to the initial lower state because both Rabi frequencies are small. At intermediate intensity, the resonant $|1\rangle \leftrightarrow |3\rangle$ transition dominates the redistribution process. At higher intensity, Ω_{32} becomes large enough for the off-resonant $|2\rangle \leftrightarrow |3\rangle$ branch to contribute appreciably. This explains why the steady-state response changes from a two-level-like redistribution pattern to a three-level population balance.

The effect of γ_{32} on this steady-state behavior is shown in Figures 3(b) and 3(c). When γ_{32} is varied while the remaining parameters are kept fixed, the overall crossover mechanism is preserved, but the stationary population partition changes because the redistribution from the upper state is redirected with different efficiencies. For larger γ_{32}, population transferred to $|3\rangle$ is more efficiently funneled into $|2\rangle$, whereas for smaller γ_{32} this route is weakened and a larger fraction of the population remains associated with, or returns through, the resonantly driven $|1\rangle \leftrightarrow |3\rangle$ branch. This behavior is consistent with the transient results discussed previously: γ_{32} primarily controls how efficiently population leaving the upper state is redirected toward $|2\rangle$. As a result, it changes the residence of population in the lower levels without fundamentally altering the mechanism by which the off-resonant channel becomes active. In other words, γ_{32} mainly determines the relaxation pathway and the steady-state balance once population has been transferred through the upper state.

A different role is played by the transition dipole moment μ_{32}, as illustrated in Figure 4. Since $\Omega_{32} = \mu_{32}E_0/\hbar$, changing μ_{32} directly modifies how rapidly the off-resonant branch becomes relevant as the field intensity increases. For a larger μ_{32}, shown in Figure 4(a), the crossover to three-level redistribution occurs at lower intensity because the effective coupling of the $|2\rangle \leftrightarrow |3\rangle$ transition is strengthened. Consequently, population transfer out of $|2\rangle$ becomes easier, and the stationary populations are redistributed more strongly at intermediate and high intensities. By contrast, for a smaller μ_{32}, as in Figure 4(b), the off-resonant branch remains weak over a broader intensity range, so the crossover is displaced toward higher intensity and the state $|2\rangle$ retains a larger share of the stationary population. The comparison between Figures 3 and 4 also clarifies why γ_{32} and μ_{32} have different physical roles. The rate γ_{32} acts after population reaches the upper state and controls how that population is redistributed through relaxation. In contrast, μ_{32} changes the optical coupling strength of the off-resonant branch through $\Omega_{32} = \mu_{32}E_0/\hbar$. Therefore, γ_{32} mainly changes the population partition, whereas μ_{32} shifts the intensity range in which the third level becomes dynamically involved.

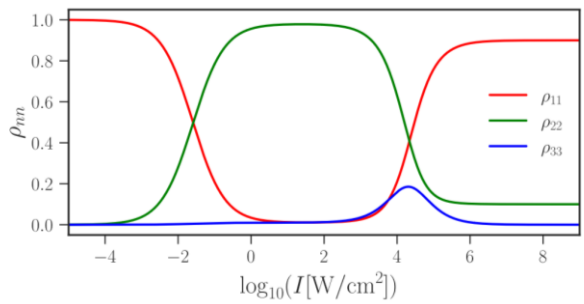

(a)

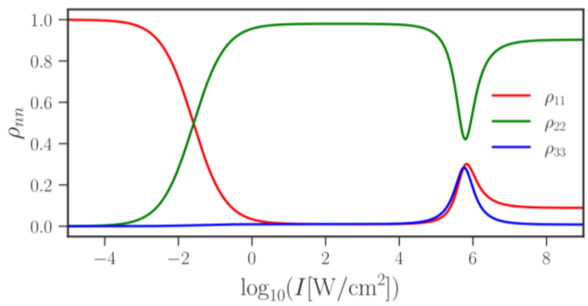

(b)

Figure 4. Steady-state populations ρ_{11}, ρ_{22}, and ρ_{33} as functions of the driving-field intensity for fixed $\gamma_{32} = \gamma_{31}$ and two representative values of the off-resonant transition dipole moment: (a) $\mu_{32} = 3\mu_{31}$ and (b) $\mu_{32} = 0.3\mu_{31}$. The calculations are carried out under resonance with the $|1\rangle \leftrightarrow |3\rangle$ transition, while the remaining parameters are fixed as specified in the text.

Taken together, the intensity-dependent results show that the stationary response is controlled by two distinct mechanisms. The parameter γ_{32} mainly regulates the relaxation route by determining how population from the upper state is partitioned between the two lower states, whereas μ_{32} mainly regulates the crossover intensity by determining how readily the off-resonant transition participates in the driven dynamics. This interpretation is broadly consistent with earlier studies showing that the driven optical response of semiconductor nanostructures is sensitive to dissipation, coupling, and excitation conditions [10,13,14]. At the same time, the present results extend that general picture by showing, for a single continuously driven Λ-type SQD, that relaxation-path asymmetry and off-resonant coupling strength play physically distinct roles: the former primarily controls the redistribution pathway and stationary population balance, whereas the latter determines the onset of effective three-level participation under increasing intensity. The combined effect of these two parameters, therefore, explains how the system evolves from a predominantly resonant two-level-like steady-state response at low intensity into a genuine three-level population redistribution regime at stronger driving, thereby providing a more explicit mechanism-based interpretation than is usually available from broader driven-response studies.

Connection with Possible Material Realizations

Although the present model is formulated in terms of effective parameters, the quantities considered here can be connected to experimentally relevant semiconductor quantum-dot platforms. Self-assembled InGaAs/GaAs and GaN/AlN quantum dots provide useful examples. Both systems support discrete excitonic transitions, and their recombination dynamics can be examined by time-resolved optical measurements [19],[23]. More generally, time-resolved photoluminescence has been widely used to analyze carrier and exciton relaxation dynamics in self-assembled quantum dots [18]. Within the present effective model, the relaxation rates should be regarded as phenomenological branch-specific population-transfer rates rather than fixed material constants. In particular, γ_{32} denotes an effective relaxation channel from the upper state $|3\rangle$ to the lower state $|2\rangle$. Its value may be influenced by the microscopic relaxation pathways available in the quantum-dot structure considered, in particular radiative recombination, nonradiative decay, and phonon-assisted relaxation [18,23-24].

The same interpretation applies to the off-resonant transition dipole moment μ_{32}. In the present model, μ_{32} the effective optical coupling strength of the $|2\rangle \leftrightarrow |3\rangle$ transition. For real semiconductor quantum dots, however, this parameter is not universal. Its value, and hence the associated oscillator strength, may depend on the confinement geometry, wave-function overlap, shape anisotropy, strain, band mixing, and the local electronic structure of the dot [23,25-26]. The predicted decrease in crossover intensity with increasing μ_{32} should therefore be interpreted, within the present model, as a mechanism-level trend rather than a material-specific prediction. For the same set of remaining parameters, a larger off-resonant transition dipole moment increases the effective coupling of the $|2\rangle \leftrightarrow |3\rangle$ branch. As a result, the system enters the three-level redistribution regime at a lower excitation intensity. If this off-resonant branch is weaker, the response remains closer to two-level-like behavior over a wider intensity interval. Changing the relaxation branching ratio, represented here by γ_{32}, has a different effect. In the parameter regime considered, it mainly changes the final population balance between the lower states. This separation of effects links the model to experimentally relevant SQD platforms without making a material-specific prediction that would require direct extraction of parameters from a particular sample.

CONCLUSION

This study has clarified the mechanism governing the time- and intensity-dependent population response of a continuously driven single Λ-type semiconductor quantum dot within the density-matrix framework under the rotating-wave approximation. The time-domain analysis shows that the additional relaxation channel γ_{32} primarily controls the transient redistribution route and the timescale for reaching the stationary regime, while the early oscillatory behavior remains dominated by the resonantly driven $|1\rangle \leftrightarrow |3\rangle$ transition. In the steady-state regime, the results reveal a clear separation of roles between the two key parameters examined. The relaxation rate γ_{32} mainly determines how population leaving the upper state is redistributed between the two lower states, whereas the dipole moment μ_{32} governs how readily the off-resonant $|2\rangle \leftrightarrow |3\rangle$ branch becomes active as the driving intensity increases. Consequently, the crossover from predominantly resonant two-level-like behavior to genuine three-level population redistribution is controlled not by a single factor, but by the combined action of relaxation-path asymmetry and off-resonant coupling strength. These findings establish a more explicit physical picture of driven population redistribution in an effective multilevel SQD model and provide a useful basis for interpreting nonequilibrium population dynamics in more complex semiconductor quantum-dot systems.

ACKNOWLEDGMENTS

This work was supported by DIPA UNTAN No. SP DIPA-023.17.2.677517/2023, contract No. 2792/UN22.8/PT.01.05/2024.

REFERENCES

[1] Feng, D., Zhang, G. & Li, Y. Semiconductor Quantum Dots: Synthesis, Properties and Applications. *Nanomaterials* vol. 14 1825 Preprint at https://doi.org/10.3390/nano14221825 (2024).
[2] Meng, L., Xu, Q., Zhang, J. & Wang, X. Colloidal quantum dot materials for next-generation near-infrared optoelectronics. *Chem. Commun.* **60**, 1072–1088 (2024).
[3] Heindel, T., Kim, J.-H., Gregersen, N., Rastelli, A. & Reitzenstein, S. Quantum dots for photonic quantum information technology. *Adv. Opt. Photonics* **15**, 613–738 (2023).
[4] Zhou, X., Zhai, L. & Liu, J. Epitaxial quantum dots: a semiconductor launchpad for photonic quantum technologies. *Photonics Insights* **1**, R07–R07 (2023).
[5] Manson, R., Roy-Choudhury, K. & Hughes, S. Polaron master equation theory of pulse-driven phonon-assisted population inversion and single-photon emission from quantum-dot excitons. *Phys. Rev. B* **93**, 155423 (2016).
[6] Poltavtsev, S. V *et al.* Damping of Rabi oscillations in intensity-dependent photon echoes from exciton complexes in a CdTe/(Cd,Mg)Te single quantum well. *Phys. Rev. B* **96**, 75306 (2017).
[7] Grisard, S. *et al.* Multiple Rabi rotations of trions in InGaAs quantum dots observed by photon echo spectroscopy with spatially shaped laser pulses. *Phys. Rev. B* **106**, 205408 (2022).
[8] Kosarev, A. N. *et al.* Extending the time of coherent optical response in ensemble of singly-charged InGaAs quantum dots. *Commun. Phys.* **5**, 144 (2022).
[9] Boos, K. *et al.* Signatures of Dynamically Dressed States. *Phys. Rev. Lett.* **132**, 53602 (2024).
[10] Moody, G. & Cundiff, S. T. Advances in multi-dimensional coherent spectroscopy of semiconductor nanostructures. *Adv. Phys. X* **2**, 641–674 (2017).
[11] Hu, X. *et al.* Photoluminescence of InAs/GaAs quantum dots under direct two-photon excitation. *Sci. Rep.* **10**, 10930 (2020).
[12] Veisi, M., Kazemi, S. H. & Mahmoudi, M. Tunneling-induced optical limiting in quantum dot molecules. *Sci. Rep.* **10**, 16304 (2020).
[13] Ryzhov, I. V., Malikov, R. F., Malyshev, A. V. & Malyshev, V. A. Nonlinear optical response of a two-dimensional quantum-dot supercrystal: Emerging multistability, periodic and aperiodic self-oscillations, chaos, and transient chaos. *Phys. Rev. A* **100**, (2019).

[14] Tohari, M. M., Alqahtani, M. M. & Lyras, A. Optical Multistability in the Metal Nanoparticle–Graphene Nanodisk–Quantum Dot Hybrid Systems. *Nanomaterials* vol. 10 1687 Preprint at https://doi.org/10.3390/nano10091687 (2020).

[15] Paspalakis, E., Smponias, A. & Stefanatos, D. Coherent preparation of the biexciton state in a semiconductor quantum dot coupled to a metallic nanoparticle. *J. Appl. Phys.* **129**, 223104 (2021).

[16] Nugroho, B. S., Iskandar, A. A., Malyshev, V. A. & Knoester, J. Plasmon-assisted two-photon absorption in a semiconductor quantum dot-metallic nanoshell composite. *Phys. Rev. B* **102**, 1–8 (2020).

[17] Löbl, M. C. *et al.* Excitons in InGaAs quantum dots without electron wetting layer states. *Commun. Phys.* **2**, 93 (2019).

[18] Man, M. T. & Lee, H. S. Clarifying photoluminescence decay dynamics of self-assembled quantum dots. *Sci. Rep.* **9**, 4613 (2019).

[19] Stachurski, J., Tamariz, S., Callsen, G., Butté, R. & Grandjean, N. Single photon emission and recombination dynamics in self-assembled GaN/AlN quantum dots. *Light Sci. Appl.* **11**, 114 (2022).

[20] Khanonkin, I., Bauer, S., Eyal, O., Reithmaier, J. P. & Eisenstein, G. Steering coherence in quantum dots by carriers injection via tunneling. *Nanophotonics* **11**, 3457–3463 (2022).

[21] Lu, X., Huang, D. & Fan, S. Effect of Coulomb interaction on the transient optical response of electrons in field-coupled quantum dots. *Phys. Rev. A* **103**, 43504 (2021).

[22] Ryzhov, I. V., Malikov, R. F., Malyshev, A. V. & Malyshev, V. A. Quantum metasurfaces of arrays of Λ-emitters for photonic nano-devices. *J. Opt. U. K.* **23**, 1–14 (2021).

[23] Große, J., Mrowiński, P., Srocka, N. & Reitzenstein, S. Quantum efficiency and oscillator strength of InGaAs quantum dots for single-photon sources emitting in the telecommunication O-band. *Appl. Phys. Lett.* **119**, 61103 (2021).

[24] Quilter, J. H. *et al.* Phonon-Assisted Population Inversion of a Single $\mathrm{InGaAs}/\mathrm{GaAs}$ Quantum Dot by Pulsed Laser Excitation. *Phys. Rev. Lett.* **114**, 137401 (2015).

[25] Barettin, D. *et al.* Optical properties and optimization of electromagnetically induced transparency in strained InAs/GaAs quantum dot structures. *Phys. Rev. B* **80**, 235304 (2009).

[26] Muller, A., Wang, Q. Q., Bianucci, P., Shih, C. K. & Xue, Q. K. Determination of anisotropic dipole moments in self-assembled quantum dots using Rabi oscillations. *Appl. Phys. Lett.* **84**, 981–983 (2004).